applied sciences

MDPI

Article

Effective Elastic Thickness in Northern South America

Ivan F. Casallas * and Jyr-Ching Hu

Department of Geosciences, National Taiwan University, Taipei 10617, Taiwan; jchu@ntu.edu.tw
* Correspondence: ivanfcasallas@gmail.com or d07224008@ntu.edu.tw

Abstract: The strength of the lithosphere plays an important role in understanding the deformation process of the Earth. In northern South America, the convergence of three tectonic plates has resulted in a zone of active deformation. The effective elastic thickness (T_e) is a parameter that serves as a proxy for the lithospheric strength. This study determined the spatial variations of T_e across northern South America through a joint inversion of admittance and coherence using Bouguer gravity anomaly and topography data. The inversion reveals that T_e ranges from 15 to 60 km, with high T_e (>50 km) corresponding to stable cratons, whereas low T_e (<20 km) is displayed in areas close to continental margins. The Colombian Andes exhibit an intermediate T_e value, ranging from 20 to 40 km. The subsurface-to-surface ratio (*F*) indicates dominant surface loading in the region. Furthermore, a correlation was observed between T_e and other proxies for lithospheric structure, such as seismic velocity.

Keywords: effective elastic thickness; lithosphere; strength; deformation; WGM2012; South America

1. Introduction

The lithosphere is the outer rigid layer of the Earth and is exposed to continuous deformation. Mechanical strength is a fundamental property of the lithosphere that controls its deformation processes in response to long-term forces [1–5]. The effective elastic thickness (T_e) of the lithosphere corresponds to the thickness of an idealized elastic beam that would bend similarly to the actual lithosphere under the same applied loads [6]. T_e can be interpreted as a proxy for the integrated strength of the lithosphere and reflects the response of the lithosphere to long-term (>10^5 yr) geological loads [7]. Oceanic T_e is mainly controlled by the thermal age and correlates well with the 450–600 °C isotherm from a cooling plate model. In contrast, continental T_e does not correspond to an isotherm or a physical boundary, and factors such as crustal thickness and flexural plate curvature also play important roles [1,6,8]. The T_e provides insight into the rheology and state of stress of the lithosphere, as well as its temporal evolution and spatial configuration, and tectonic styles [2,9,10].

Various methodologies have been developed to compute T_e, with the most prevalent being forward modeling and spectral methods. In forward modeling, predictions of gravity or topography are compared directly with those of elastic plate models [7]. Spectral methods, particularly admittance and coherence, find the statistical relationship between gravity and topography in the frequency domain, estimating T_e by inverting these spectral measures against a theoretical plate model [11]. The admittance is a wavenumber-domain transfer function that enables gravity to be predicted from topography, whereas the coherence is a measure of the phase relationship between two signals [12]. Traditionally, the oceanic T_e is calculated using the admittance method and free air anomaly. By contrast,

check for updates

Academic Editor: Fernando Rocha

Received: 1 April 2025
Revised: 2 May 2025
Accepted: 3 May 2025
Published: 6 May 2025

Citation: Casallas, I.F.; Hu, J.-C. Effective Elastic Thickness in Northern South America. *Appl. Sci.* **2025**, *15*, 5163. https://doi.org/10.3390/app15095163

Copyright: © 2025 by the authors. Licensee MDPI, Basel, Switzerland. This article is an open access article distributed under the terms and conditions of the Creative Commons Attribution (CC BY) license (https://creativecommons.org/licenses/by/4.0/).

the estimation of continental T_e has been a topic of continuous debate. Initial estimations of continental T_e employed the admittance method and free air gravity anomaly, assuming only surface loading, and retrieving low T_e values where higher values were expected [13,14]. Forsyth [15] addressed this issue by including surface and subsurface loads (e.g., igneous intrusions, magmatic underplating) and using the Bouguer coherence function. However, McKenzie and Fairhead [16] and McKenzie [17] disputed Forsyth's [15] approach, arguing that it provided upper bounds rather than a true estimation of continental T_e. Despite the debate, the Bouguer coherence method remains widely used for T_e in the continental lithosphere.

Northern South America is a tectonically complex region encompassing processes such as subduction, collision, and active volcanism. Consequently, the estimation of the T_e provides information that contributes to the understanding of this tectonic setting. In the past, numerous studies on T_e across northern South America have been conducted employing diverse datasets and methodologies; however, a detailed image of the spatial variation of T_e in this region remains lacking. For instance, Tassara et al. [2], Pérez-Gussinyé et al. [18], and Jiménez-Díaz et al. [19] utilized the Bouguer coherence to map the spatial variations of T_e in South America and surrounding areas. Stewart and Watts [20] and Galán and Casallas [21] calculated an average T_e for the Colombian Cordillera system. Additionally, Ojeda and Whitman [22] employed the multitaper method to determine the average T_e for three subareas in northern South America.

In this study, we determined the spatial variations of T_e in northern South America following the approach of Audet [23]. For this purpose, a joint inversion of real Bouguer admittance and coherence using wavelet transform and incorporating combined loading (surface and subsurface) was performed using global gravity anomalies and topography data [23,24]. Subsequently, we interpreted the T_e distribution in a tectonic context and examined the relationship between the spatial variations of T_e and other proxies for lithospheric structure, contributing to the understanding of the lithosphere in this region.

2. Tectonic Setting

In northern South America, a complex interaction exists among the Caribbean, Nazca, and South American Plates (Figure 1). The Caribbean plate is converging obliquely in an east-southeastward direction at a rate of 17.0 ± 0.4 mm/yr., while the Nazca plate converges east-northeastward at a rate of 53.1 ± 0.6 mm/yr., both relative to the stable South American Plate [25]. The stress generated by this triple junction is accommodated by the Panama-Choco and North Andean Blocks [26,27]. This region is composed of a combination of terranes accreted to the Guiana Shield at various times from late Paleozoic through Middle Miocene [28].

The Panama-Choco Block (PCB) is a volcanic arc accompanied by oceanic crust, formed on the edge of the Caribbean Plate and related to the subduction of the Farallon Plate, and later the Cocos Plate [28,29]. It collides into northern South America in a E-SE direction, but without subducting it, because of its buoyancy [30,31]. This collision is considered responsible for the uplifting in the Colombian Andes which affected the three cordilleras [30–32]. Trenkamp et al. [33] and Suter et al. [31] proposed that PCB acts as a rigid indenter.

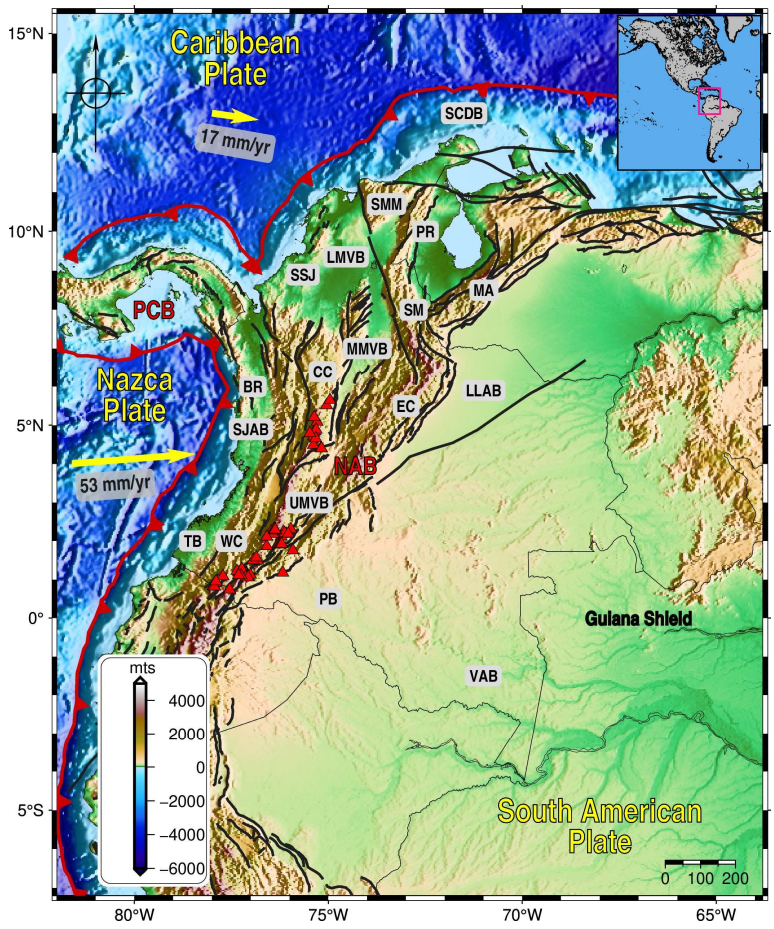


Figure 1. Tectonic setting and topography of northern South America. Velocity vectors from Mora-Páez et al. [25] and major faults from Veloza et al. [34]. Major tectonic structures as follows: SCDB: South Caribbean Deformation Belt, SMM: Santa Marta Massif, SSJ: Sinú-San Jacinto belts, LMVB: Lower Magdalena Valley Basin, PR: Perija Range, BR: Baudó Range, CC: Central Cordillera, MMVB: Middle Magdalena Valley Basin, SM: Santander Massif, MA: Merida Andes, SJAB: San Juan-Atrato Basin, EC: Eastern Cordillera, LLAB: Llanos Basin, TB: Tumaco Basin, WC: Western Cordillera, UMVB: Upper Magdalena Valley Basin, PB: Putumayo Basin, VAB: Vaupes-Amazonas Basin, PCB: Panama-Choco Block, NAB: North Andean Block. Red triangles represent active volcanoes.

The North Andean Block (NAB) is an independent and distinct geologic segment of the Andean Cordillera, moving at a rate of 8.6 mm/yr. toward N60°E direction relative to the rest of South America and being compressed in an E-W direction [25,35–37]. In Colombia, the Andean Belt is segmented into three mountain systems: the Eastern, the Central and the Western Cordilleras. The Eastern Cordillera is an intracontinental belt, oriented NE and composed of a Precambrian and Paleozoic polymetamorphic basement, covered by a sequence of Cretaceous sedimentary rocks and bounded by major inverse faults [27]. The Central Cordillera has a low-grade polymetamorphic Triassic basement that includes oceanic and continental rocks, intruded by Cenozoic plutons generated by the subduction of the Nazca plate under the South American plate. The Central Cordillera is limited by reverse fault systems located along the foothills, which root beneath the range. The Western Cordillera is a basic Igneous complex constituted by basaltic rocks of the Caribbean-Colombian oceanic plateau, accreted during Mesozoic and early Cenozoic. The Western Cordillera is characterized by thrust and fold during late Cenozoic, associated to the Nazca subduction and the accretion of Caribbean blocks [30,38,39]. In the northernmost Andes of Colombia is the Santa Marta Massif (SMM), a triangular pyramidal isolated block, fault-bounded, and surrounded by Cenozoic basins; which is composed by Jurassic

magmatic rocks, Paleozoic schists, and allochthonous Late Cretaceous amphibolites [40,41]. The bounding structures of the Santa Marta Massif represent significant structures along the southern Caribbean plate boundary [42].

The Colombian Caribbean Margin is a consequence of the E-NE migration of the Caribbean plate and its subsequent subduction beneath Colombia, resulting in the identification of three structural provinces: the Sinú Fold Belt, the San Jacinto Fold Belt, and the Lower Magdalena Valley Basin [43]. The Sinú and San Jacinto Fold belts form an accretionary wedge of sediments up to 12 km thick which has been accreted to NW Colombian margin during Cenozoic [44]. These two belts are separated by the Sinú Fault. The Sinú Fold Belt presents mud diapirism or mud volcanoes, a feature devoid in the San Jacinto Fold Belt [45]. The Lower Magdalena Valley Basin is a forearc basin situated between the Central Cordillera and the Sierra Nevada de Santa Marta [46]. The Lower Magdalena Valley Basin is composed of Permian-Triassic metasedimentary rocks and is considered the northward continuation of the basement terranes of the Northern Central Cordillera [47]. Below the Lower Magdalena Valley Basin, the subducted slab has an initial dip of 4–8° which increases to 30–50° at a distance of 200 km from the frontal thrust of the Southern Caribbean Deformation Belt. This shallow dip may serve as the mechanism for uplifting of the basin [48].

The Amazonian Craton, one of the largest cratonic areas in the world, forms a part of the crystalline core of the South American continent. It is divided into two provinces by the Amazonas sedimentary basin: Guiana Shield to the north and Central Brazilian Shield [49,50]. In Colombia, the Amazonian Craton extends from the eastern flank of the Andean Cordillera in the Llanos Foothills to the borders with Venezuela, Brazil, and Perú [51]. This region encompasses the Llanos, Putumayo, and Vaupés-Amazonas Basins. The basement of the Amazonian Craton in Colombia (mostly covered by a thick sedimentary cover) is formed by Precambrian igneous, metamorphic, and sedimentary rocks of the western Guiana Shield [52].

3. Data and Methodology

We estimate the spatial variation of T_e in northern South America by a joint inversion of real Bouguer admittance and coherence [23]. The spectral admittance and coherence functions are defined by [24]:

$$Z(k) = \frac{\langle G(k)H^*(k)\rangle}{\langle H(k)H^*(k)\rangle} \quad (1)$$

$$\gamma^2(k) = \frac{|\langle G(k)H^*(k)\rangle|^2}{\langle G(k)G^*(k)\rangle \langle H(k)H^*(k)\rangle} \quad (2)$$

where $G(k)$ and $H(k)$ are the gravity and topography spectra respectively. k is the two-dimensional wavenumber, and $k = |k| = \sqrt{k_x^2 + k_y^2}$, where k_x, k_y, are the wavenumbers in x and y directions. The asterisk indicates complex conjugation, and brackets indicate an averaging procedure. The spectra are calculated using the continuous planar wavelet transform (CWT) with a Fan wavelet [53], which is a superposition of 2D Morlet wavelets with different azimuths spanning 180° [11,54]. The central wavenumber $|k_0|$ of the Morlet wavelet governs its spatial–spectral resolution. We set $|k_0| = 5.336$ to satisfy the zero-mean requirement of the wavelets, which provides a more accurate absolute T_e estimation, but the spatial resolution decreases. In contrast, a low $|k_0|$ provides a better resolution, but the uncertainty on the estimation of T_e increases [54].

The predicted admittance and coherence are calculated using the "uniform-f" method [23], in which the subsurface-to-surface load ratio, f, and T_e are independent and adjustable parameters during the inversion [55]. Following Forsyth [15], the subsurface load is emplaced at the Moho which is characterized by a marked density contrast. The

ratio of the internal to the total load is defined by $F = f/(1 - f)$ [17]. $F = 0$ reflects a purely surface loading, while $F = 1$ indicates a dominant subsurface loading and $F = 0.5$ equals combined loading [11,56]. The values of T_e and F are estimated by jointly minimizing the misfit between observed and predicted admittance and coherence [24]. The misfit is calculated using a reduced chi-squared criterion [23]:

$$\chi^2(F, T_e) = \frac{1}{(2N-2)} 2\sum_{i=1}^{N} \left(\frac{d_{ij} - S_{ij}(F, T_e)}{\sigma_{ij}} \right)^2 \quad (3)$$

where d_{ij} is the i^{th}measured sample of either real admittance or coherence with variance ${\sigma_{ij}}^2$, S_{ij} the analytical quantity for a given model, and N is the number of samples.

In this study, topographic data (Figure 1) were obtained from the ETOPO1 digital elevation model, which has a spatial resolution of 1 arc-minute [57]. The Bouguer anomaly data (Figure 2) were extracted from WGM2012, an earth gravity anomaly model computed at a global scale in spherical geometry that considers the contribution of most surface masses [58] and has a spatial resolution of $2' \times 2'$. The thickness (Figure 3a) and density (Figure 3b) of the crust were derived from the CRUST1.0 model [59]. All geographical grids were transformed into Cartesian coordinates using the Mercator projection and gridded at a 5×5 km^2 cell size. To mitigate the boundary effects, the grid was extended by 3° beyond the study area, which is the Colombian territory.

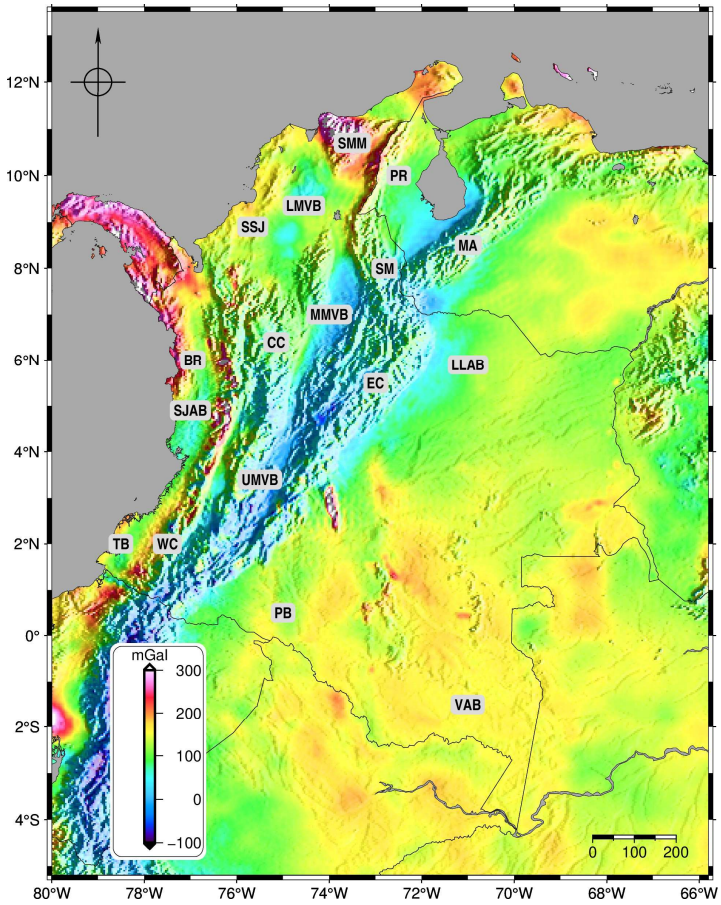


Figure 2. Bouguer gravity anomaly over northern South America. Data from WGM2012 global gravity model [58]. The annotations are the same as in Figure 1.

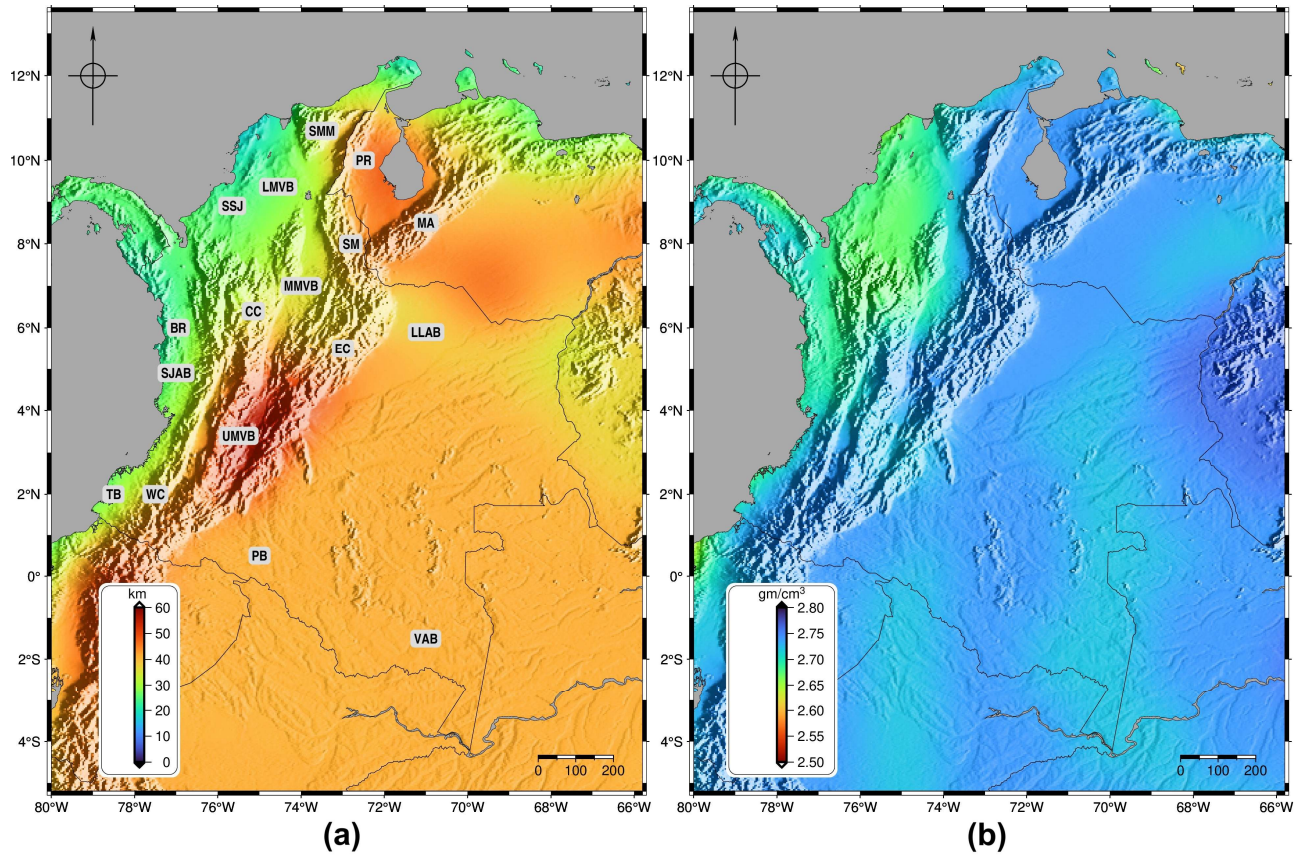


Figure 3. Crustal structure over northern South America. (**a**) Crustal thickness. (**b**) Density crustal. Data from CRUST1.0 [59]. The annotations are the same as in Figure 1.

4. Results and Discussion

4.1. Spatial Variation of T_e and Loading Ratio (F)

From a broad view, the map of spatial variation of T_e in Colombia (Figure 4a) reveals that the T_e varies between 15 km at the southern flank of the Colombian Pacific margin and 60 km in the Amazonian Craton. Additionally, an increasing trend of T_e in W-E direction is observed. The *F* value is predominantly low (*F*~0.2) across the region, indicating that the surface loading is dominant (Figure 4b). This type of loading is caused by topography and large-scale variations in surface density [19]. This aligns with the tectonic setting, that is dominated by mountain ranges and sedimentary basins. The uncertainties in T_e (<5 km) (Figure 5a) and *F* (<0.10) (Figure 5b) are small, showing the robustness of the results using the joint inversion of admittance and coherence.

The findings indicate that within the Caribbean Colombian margin, the Guajira Peninsula and the Lower Magdalena Valley Basin (LMVB) exhibit a variation in T_e from 40 to 45 km, whereas beneath the Santa Marta Massif (SMM), the T_e ranges from 25 (at the NW flank) to 43 km. In relation to the Sinú and San Jacinto Fold belts (SSJ), both are characterized by a T_e of 30–40 km. Comparing these T_e variations with seismic tomography studies, Poveda et al. [60,61] reported a lithospheric thickness of approximately 30 km under Sinú and San Jacinto belts (SSJ), approximately 35 km beneath Lower Magdalena Valley Basin (LMVB), and about 40 km under Santa Marta Massif (SMM), which indicates a positive correlation with the T_e estimations. The T_e lateral variations suggest a relatively strong lithosphere, reflecting the tectonic features of this area. The T_e value obtained for Santa Marta Massif (SMM) supports the idea that a rigid lithosphere could provide mechanical support to the topography; nonetheless, it is unable to explain the positive Bouguer gravity anomaly meaning the lack a crustal root [62].

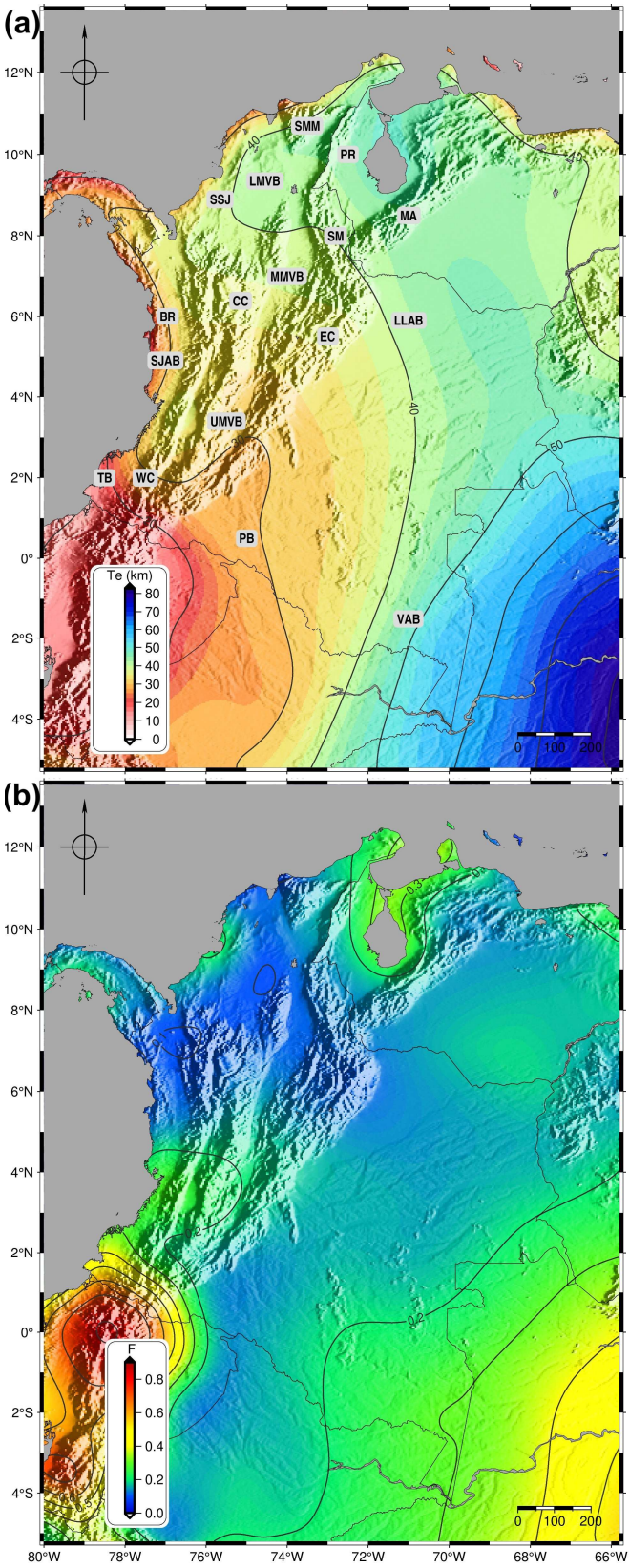


Figure 4. Results obtained from the joint inversion of real Bouguer admittance and coherence over northern South America. (**a**) Effective elastic thickness (T_e). (**b**) Load ratio *F*. The annotations are the same as in Figure 1.

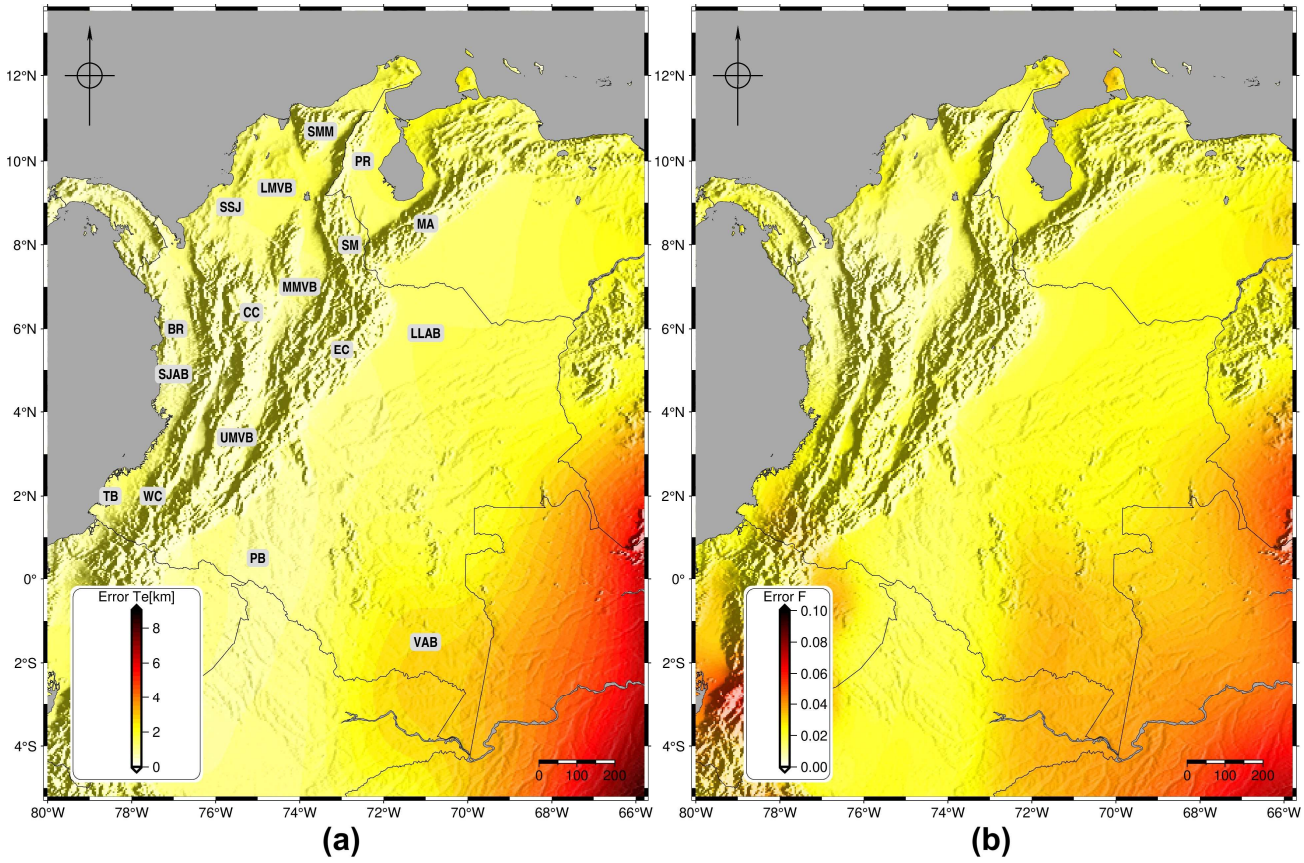


Figure 5. Errors obtained from the joint inversion of real Bouguer admittance and coherence over northern South America. (**a**) Effective elastic thickness (T_e). (**b**) Load ratio *F*. The annotations are the same as in Figure 1.

Over the Colombian Pacific margin, the T_e ranges between 15 and 30 km in the Tumaco Basin (TB), whereas a uniform value of 35 km is observed in the San Juan and Atrato Basins (SJAB). The Baudó Range (BR), a narrow band situated to the east of the Atrato Basin, has T_e of 25–35 km. The lowest value (15 km) on the southernmost flank is shared by a portion of the Tumaco Basin and the southern volcanic center of Colombia, and it continues to extend throughout the Ecuadorian territory. This volcanic center corresponds to the continuation of the Ecuadorian volcanism, which extends over a broad region from the Western Cordillera to the Subandean Zone in Ecuador [63,64]. This region is characterized by active volcanism and geothermal systems, magma reservoirs, and partial melt [64–67], and exhibits low seismic velocity [61,67,68], indicating a relatively hot lithosphere and, consequently, low flexural rigidity [18,19]. This reduction in lithospheric strength is indicative of subduction-related volcanism within the cordillera [69]. These low T_e values are common in deforming regions of active subduction [70].

The Colombian Cordilleras are characterized by T_e values ranging from 20 to 40 km. Overall, there is a positive correlation between crustal thickness studies using seismic tomography [60,61,71] and gravity data [72], which report crustal thickness values between 30 and 60 km. Across the entire Cordillera system, the lower T_e values are located on the southern flank, increasing smoothly towards the north, where the thickest T_e (40 km) is found in the Eastern Cordillera (EC), which bifurcates into the Merida Andes (MA) and Perija Range (PR) (Venezuela). Research conducted by Mojica Boada et al. [71] and Poveda et al. [60,61] also reported crustal thickening in the northern part of the Cordilleran system, particularly in the Eastern Cordillera (EC), where the crustal thickness beneath the northernmost section is approximately 60 km. This crustal thickening has been linked

to a process of tectonic shortening and a more rigid lithospheric behavior in the northern segment than in the southern segment [73]. The Middle Magdalena Valley Basin Valley (MMVB), which separates the Central (CC) from the Eastern Cordillera (EC) has a T_e ranging from 35 to 40 km.

The Amazonian Craton in Colombia exhibits a T_e ranging from 25 to 60 km. In the Putumayo Basin (PB), the T_e varies between 25 and 35 km. Further northeast, in the Llanos Basin (LLAB), the T_e increases to 45 km; consistent with the presence of the Precambrian basement of the Guiana Shield along its eastern margin [74]. In the Putumayo Basin (PB), the variation in T_e, results from its location within a transition zone between flat to steeper-dipping subduction slab [75]. Toward the southern Colombian territory, in the area approximately covered by the Vaupés-Amazonas Basin (VAB), the T_e varies from 30 to 60 km, with the highest T_e found in the southernmost tip (the boundary Colombia, Perú, and Brasil), an area potentially connected with the intracratonic Brazilian basin of Solimões [76] and characterized by high seismic velocities [77,78].

In examining the two tectonic blocks, it is observed that the Panama-Choco Block (PCB) has a $T_e < 30$ km, whereas the adjacent North Andean Block (NAB) exhibits a $T_e > 40$ km. This disparity in T_e values is interesting, because assuming that the PCB acts as a rigid indenter [31,33] or as a broken indenter [25], causing deformation and uplift of the Northern Andes, a higher T_e compared to that of NAB would be expected. The low T_e value observed in PCB may be elucidated by the model proposed by Rockwell et al. [79], which characterizes this tectonic block as a soft block indenter with considerable internal deformation. Nonetheless, further comprehensive investigations are required to determine this aspect.

4.2. Comparison with Previous Results

Several estimations of T_e have been conducted for northern South America. The studies by Tassara et al. [2], Pérez-Gussinyé et al. [18] and Jiménez-Díaz et al. [19] employed spectral techniques and global gravity models to generate maps of T_e spatial variations across the entire South American continent, yielding values for the northern region ranging from 15 to 70 km. These studies reported the highest T_e values in craton areas; which is in agreement with the findings of this study. Mantovani et al. [80,81] also determined the T_e for South America using an empirical correlation between tidal gravity anomaly and T_e. They reported a T_e range of 60 to 70 km for northern South America. This T_e value is significantly higher compared to the estimates provided by other studies. Nonetheless, Pérez-Gussinyé et al. [18] argued that the estimations by Mantovani et al. [80,81] are unlikely to be comparable with those derived from topography and gravity data, because the response of the lithosphere to this short-term cyclical stress (tidal loading) is quite different to that of long-term geological processes.

Other studies on T_e have been conducted in specific places, and their findings are consistent with our results. Stewart and Watts [20] analyzed profiles of gravity to estimate the T_e by forward modelling in the Colombian mountain range, obtaining a T_e value of 45 km. Galán and Casallas [21] estimated a T_e of 20 km for the Colombian Andes using Free air gravity anomalies profiles and the admittance technique. Ojeda and Whitmann [22] studied the T_e of Eastern Cordillera (EC) using multitaper estimators (to calculate Bouguer coherence) obtaining a value of 30 km. Using flexural analysis, Cerón et al. [82] reported a T_e of approximately 27 km for the Plato Basin, located north of the Lower Magdalena Valley Basin (LMVB). In the Putumayo Basin (PB), Londoño et al. [83] performed flexural modeling and found a T_e of 30 km, whereas Pachón-Parra et al. [75] conducted 3D flexural modeling and obtained a T_e ranging from 25 to 35 km.

Finally, comparing worldwide studies by Audet and Bürgmann [10] and Lu et al. [84], which derived T_e from Bouguer coherence and admittance using the continuous wavelet transform; and the study by Tesauro et al. [85] which calculated T_e based on the lithospheric strength distribution; reveals that our findings are in good agreement with these investigations.

4.3. T_e, Surface Heat Flow, and Seismic Velocity

The heat flow serves as an indicator of the thermal state of the lithosphere, which in turn affects the value of T_e [1,86]. Seismic velocities depend on the temperature and rock composition, factors that influence rheology, and ultimately the integrated strength of the lithosphere [18]. Several investigations have shown a correlation between the heat flow and seismic velocity with the T_e [18,24,87]. In this study, these relationships are examined for northern South America. It is important to note, however, that aspects such as the resolution of the models or that the sensitivities of seismic velocities and T_e differ and require careful comparison [18].

Figure 6a illustrates the variations in heat flow across northern South America obtained by Lucazeau [88]. The heat flow values range from 40 to 160 mW/m^2. Generally, the highest heat flow values ($\geq$120 mW/m^2) are observed in the southern volcanic segment and certain locations within the Central (CC) and Western Cordilleras (WC). Conversely, the lowest heat flow values (~45 mW/m^2) are found in some areas of Vaupés-Amazonas Basin (VAB) and the Colombia-Panamá border. The majority of the territory is dominated by relatively intermediate heat flow values (60–70 mW/m^2). A comparison of the spatial heat flow distribution in relation to T_e variation indicates that regions with high heat flow are associated with low and moderate T_e values, whereas most areas with high T_e tend to correspond to low heat flow values.

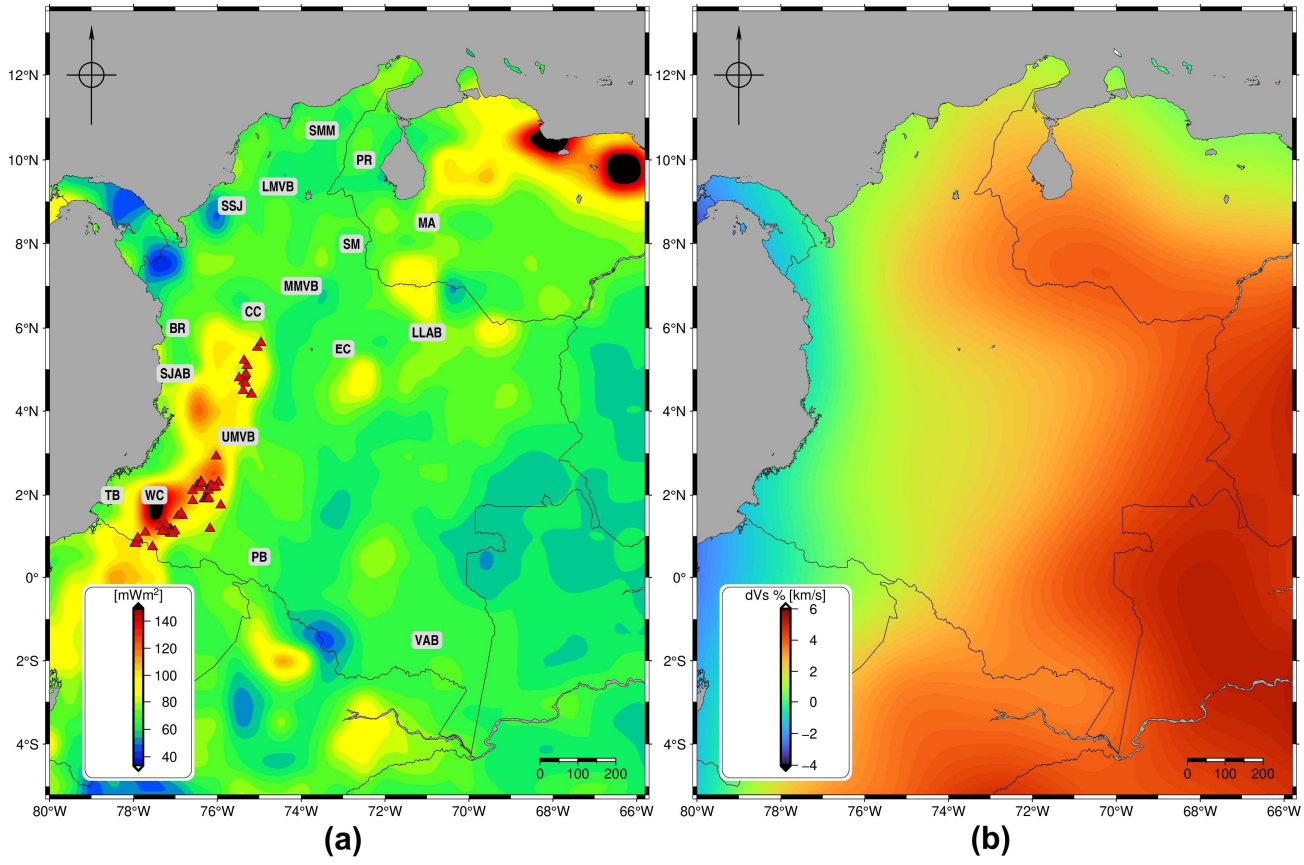


Figure 6. (**a**) Heat flow map [88] and (**b**) shear wave velocity anomaly (at 100 km depth) [89] map for northern South America. The annotations are the same as in Figure 1.

Research has demonstrated a correlation between T_e and seismic velocity anomalies at 100 km [10,18,24]. We use shear wave velocity perturbations (ΔV_s) at a depth of 100 km extracted from 3DLGL2022-TEPSv, a model developed by Debayle et al. [89], to compare them with the T_e pattern across northern South America. Overall, the resulting map of ΔV_s (Figure 6b) correlates positively with T_e. Both the velocity seismic perturbations and T_e seem to have a similar trend and direction of increase; regions with low T_e correspond to low-velocity anomalies, whereas areas with high T_e exhibit high-velocity perturbations.

In a comparative analysis of T_e, heat flow and seismic velocities, it is generally observed that regions with high T_e such as the southernmost point of Vaupés-Amazonas Basin (VAB), also exhibit high seismic velocity and low heat flow. However, the correlation between high heat flow, low seismic velocity, and low T_e, as identified in other studies [18,70], remains unclear in the context of northern South America, as shown by the fact that in the Panama zone, the T_e (Figure 4a), heat flow (Figure 6a), and seismic velocity (Figure 6b) are low.

4.4. T_e and Seismicity

Studies have shown that variations in T_e may be related to the spatial distribution of earthquakes [9,10]; because the strength contrast occurring in the lithosphere could control the localization of deformation resulting of tectonic forces and possibly the distribution of earthquakes [2]. It is worth noting that this potential correlation is a topic of continuous debate [7,90,91], necessitating careful analysis. By utilizing the T_e map and seismic activity data, this relationship within continental lithosphere is examined in the study area.

Figure 7 presents a comparison of the spatial variation of T_e with the distribution of focal depths of shallow earthquakes in the continental lithosphere ($\leq$50 km depth). The seismicity database is from the International Seismological Center Catalogue [92] for the period 1900–2023, and magnitudes between 3.0 and 7.3. We observe that seismic activity is predominantly concentrated in the Colombian Andes, with a limited number of earthquakes in the Amazonian Craton. A significant proportion of seismic activity (approximately 85%) is observed in regions where T_e is less than 40 km (Figure 8a). The majority of earthquakes (approximately 70%) are generated at depths of 0–20 km (Figure 8b). These observations indicate the absence of a direct relationship between the T_e values and focal depths of the earthquakes. Furthermore, seismic activity is located in areas with relatively intermediate T_e values (30–40 km) (Figure 8a), contrasting with the findings of Pérez-Gussinyé et al. [70] that suggest that most seismic activity tends to occur in regions with low T_e (less than 20 km). No particular relationship between T_e and subsurface loading is observed, as indicated by Tassara et al. [2]. Additionally, no increase in seismic activity is detected in areas with large T_e gradients, contrary to the study by Jiménez-Díaz et al. [19]. However, the results are consistent with the studies of Audet and Bürgmann [10] and Chen et al. [93], which state that most of the seismic activity is concentrated in regions where $T_e < 40$ km, and with Tesauro et al. [85], which reported that crustal seismicity predominantly occurs in regions with topography exceeding 1000 m and $T_e < 30$ km. Agurto-Detzel et al. [91] also investigated the relationship between T_e and seismicity, revealing that in eastern South America, areas with lower elastic thickness, $T_e < 30$ km, tend to have higher seismicity rates, whereas lower seismicity rates are associated with high T_e values ($T_e > 100$ km), which is in agreement with our findings in northern South America.

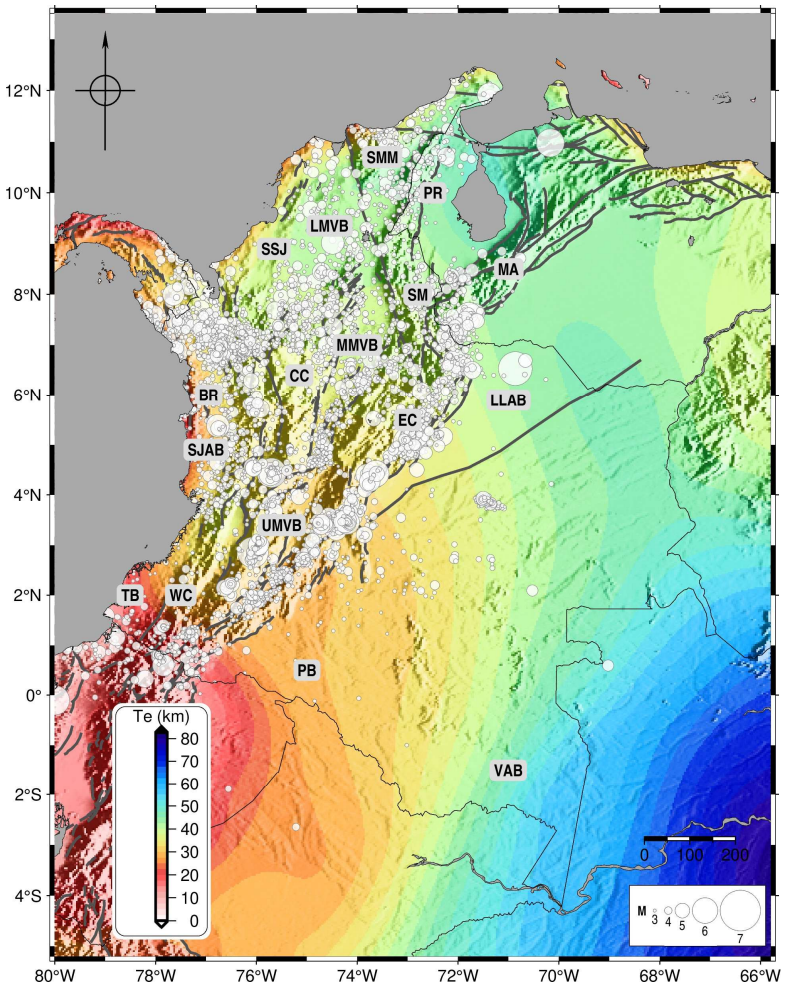


Figure 7. Distribution of the shallow seismicity (≤50 km depth) and T_e for northern South America. Seismicity from International Seismological Center Catalogue [92] for the period 1900–2023. The annotations are the same as in Figure 1.

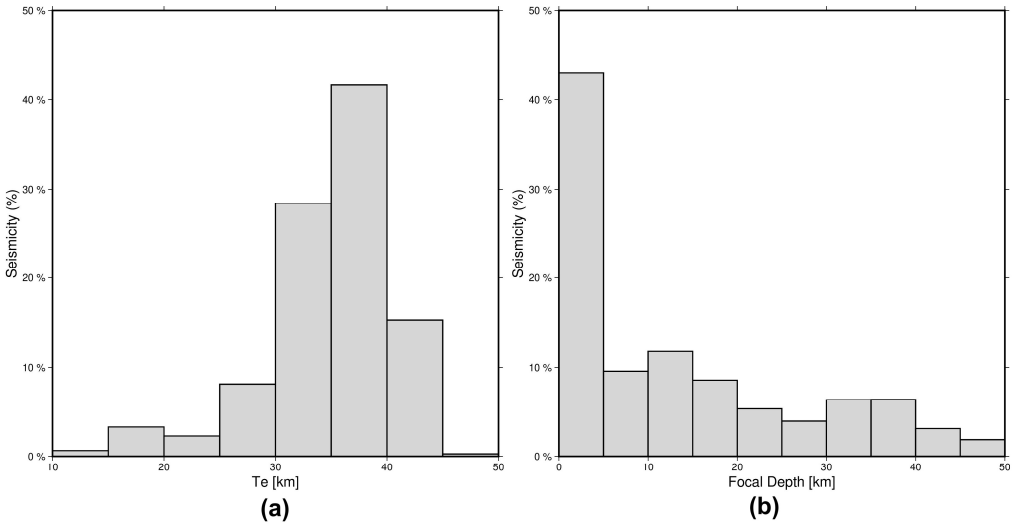


Figure 8. (**a**) Histogram showing seismicity versus T_e in northern South America. (**b**) Histogram showing seismicity versus focal depths, for the same region. Seismicity from International Seismological Center Catalogue [92] for the period 1900–2023.

Whereas T_e reflects the long-term integrated strength of the lithosphere, the seismogenic thickness (T_s) reflects the strength of the uppermost crust on historical time scales [94].

In general, T_e does not correspond to a physical depth, but it is representative of the depth to the base of Mechanical Boundary layer, which can be defined by the depth to an isotherm of the brittle–ductile transition, or by the depth at which the yielding stress or its vertical gradient become less than a particular value [4]. Thus, the shallow, brittle, and seismogenic layer is enclosed in the elastic lithosphere (i.e., $T_s < T_e$). Aligned with this, some investigations have indicated that T_e is generally greater than T_s. In the continents, T_s ranging from 0 to 25 km, whereas the T_e is in the range 0–80 km [6,7]. Although T_s has not been estimated for northern South America (it is beyond the scope of this study), it is noteworthy that most earthquakes in this region are confined to depths between 0 and 20 km, and the T_e is predominantly constrained to values exceeding 30 km.

5. Conclusions

In this study, the lithospheric strength in northern South America is investigated. For this purpose, a joint inversion of coherence and admittance, based on topography and Bouguer gravity anomaly data, was conducted. In this region, the T_e ranges from 15 to 60 km, displaying an increase in the west to east direction. The surface loading (F) is predominant in the region. The lowest T_e value (15 km) is located at the North Ecuadorian-South Colombian border, whereas the highest T_e value (60 km) is found in the southernmost tip of the Colombian territory. The Colombian Mountain range, as well as several basins, are characterized by intermediate T_e values (20–40 km). Most of the seismic activity analyzed occurred in areas where the $T_e < 40$ km. A correlation between T_e and seismic velocity was identified. Furthermore, from the analysis of the large-scale T_e pattern with heat flow and seismic velocities, it is found that tectonic stable regions are characterized by high T_e and seismic velocities but low heat flows. In general, the spatial distribution of T_e corresponds to the tectonic setting of northern South America.

Author Contributions: Conceptualization, I.F.C. and J.-C.H.; methodology, I.F.C. and J.-C.H.; software, I.F.C.; validation, I.F.C. and J.-C.H.; formal analysis, I.F.C.; investigation, I.F.C.; resources, J.-C.H.; data curation, I.F.C.; writing—original draft preparation, I.F.C.; writing—review and editing, I.F.C. and J.-C.H.; visualization, I.F.C.; supervision, J.-C.H.; project administration, J.-C.H.; funding acquisition, J.-C.H. All authors have read and agreed to the published version of the manuscript.

Funding: This research was supported by the National Science and Technology Council of Taiwan under Grant 112-2116-M-002-016.

Institutional Review Board Statement: Not applicable.

Informed Consent Statement: Not applicable.

Data Availability Statement: The WGM2012 gravity model [58] is available at https://bgi.obs-mip.fr/grids-and-models-2 (accessed on 25 June 2024). ETOPO1 [57] model is available at https://www.ncei.noaa.gov/products/etopo-global-relief-model (accessed on 25 June 2024). CRUST1.0 model [59] available at https://igppweb.ucsd.edu/~gabi/crust1.html (accessed on 25 June 2024). The elastic thickness estimations were performed using the open-source software PlateFlex v0.1.0 [95], available at https://github.com/paudetseis/PlateFlex (accessed on 9 July 2024).

Acknowledgments: The authors express sincerely thanks to the journal editors and anonymous reviewers for their comments that improved the manuscript. The figures were prepared by using Generic Mapping Tools software v 6.3 [96].

Conflicts of Interest: The authors declare no conflicts of interest.

References

1. Burov, E.B.; Diament, M. The effective elastic thickness (T_e) of continental lithosphere: What does it really mean? *J. Geophys. Res. Solid Earth* **1995**, *100*, 3905–3927. [CrossRef]

2. Tassara, A.; Swain, C.; Hackney, R.; Kirby, J. Elastic thickness structure of South America estimated using wavelets and satellite-derived gravity data. *Earth Planet. Sci. Lett.* **2007**, *253*, 17–36. [CrossRef]
3. Karato, S. *Deformation of Earth Materials: An Introduction to the Rheology of Solid Earth*; Cambridge University Press: Cambridge, UK, 2008. [CrossRef]
4. Artemieva, I. *The Lithosphere: An Interdisciplinary Approach*; Cambridge University Press: Cambridge, UK, 2011. [CrossRef]
5. Burov, E.B. Rheology and strength of the lithosphere. *Mar. Pet. Geol.* **2011**, *28*, 1402–1443. [CrossRef]
6. Watts, A.B. *Isostasy and Flexure of the Lithosphere | Solid Earth Geophysics*, 1st ed.; Cambridge University Press: Cambridge, UK, 2001.
7. Watts, A.B.; Burov, E.B. Lithospheric strength and its relationship to the elastic and seismogenic layer thickness. *Earth Planet. Sci. Lett.* **2003**, *213*, 113–131. [CrossRef]
8. Audet, P.; Mareschal, J.-C. Wavelet analysis of the coherence between Bouguer gravity and topography: Application to the elastic thickness anisotropy in the Canadian Shield. *Geophys. J. Int.* **2007**, *168*, 287–298. [CrossRef]
9. Lowry, A.R.; Smith, R.B. Strength and rheology of the western U.S. Cordillera. *J. Geophys. Res. Solid Earth* **1995**, *100*, 17947–17963. [CrossRef]
10. Audet, P.; Bürgmann, R. Dominant role of tectonic inheritance in supercontinent cycles. *Nat. Geosci.* **2011**, *4*, 184–187. [CrossRef]
11. Kirby, J. *Spectral Methods for the Estimation of the Effective Elastic Thickness of the Lithosphere, Advances in Geophysical and Environmental Mechanics and Mathematics*; Springer International Publishing: Cham, Switzerland, 2022. [CrossRef]
12. Kirby, J.F. Estimation of the effective elastic thickness of the lithosphere using inverse spectral methods: The state of the art. *Tectonophysics* **2014**, *631*, 87–116. [CrossRef]
13. Lewis, B.T.R.; Dorman, L.M. Experimental isostasy: 2. An isostatic model for the U.S.A. derived from gravity and topographic data. *J. Geophys. Res. (1896-1977)* **1970**, *75*, 3367–3386. [CrossRef]
14. Banks, R.J.; Parker, R.L.; Huestis, S.P. Isostatic Compensation on a Continental Scale: Local Versus Regional Mechanisms. *Geophys. J. Int.* **1977**, *51*, 431–452. [CrossRef]
15. Forsyth, D.W. Subsurface loading and estimates of the flexural rigidity of continental lithosphere. *J. Geophys. Res. Solid Earth* **1985**, *90*, 12623–12632. [CrossRef]
16. McKenzie, D.; Fairhead, D. Estimates of the effective elastic thickness of the continental lithosphere from Bouguer and free air gravity anomalies. *J. Geophys. Res. Solid Earth* **1997**, *102*, 27523–27552. [CrossRef]
17. McKenzie, D. Estimating T_e in the presence of internal loads. *J. Geophys. Res. Solid Earth* **2003**, *108*, 1–21. [CrossRef]
18. Pérez-Gussinyé, M.; Lowry, A.R.; Watts, A.B. Effective elastic thickness of South America and its implications for intracontinental deformation. *Geochem. Geophys. Geosystems* **2007**, *8*, 1–22. [CrossRef]
19. Jiménez-Díaz, A.; Ruiz, J.; Pérez-Gussinyé, M.; Kirby, J.F.; Álvarez-Gómez, J.A.; Tejero, R.; Capote, R. Spatial variations of effective elastic thickness of the lithosphere in Central America and surrounding regions. *Earth Planet. Sci. Lett.* **2014**, *391*, 55–66. [CrossRef]
20. Stewart, J.; Watts, A.B. Gravity anomalies and spatial variations of flexural rigidity at mountain ranges. *J. Geophys. Res. Solid Earth* **1997**, *102*, 5327–5352. [CrossRef]
21. Galán, R.; Casallas, I. Determination of effective elastic thickness of the Colombian Andes using satellite-derived gravity data. *Earth Sci. Res. J.* **2010**, *14*, 7–16. [CrossRef]
22. Ojeda, G.Y.; Whitman, D. Effect of windowing on lithosphere elastic thickness estimates obtained via the coherence method: Results from northern South America. *J. Geophys. Res. Solid Earth* **2002**, *107*, ETG 3-1–ETG 3-12. [CrossRef]
23. Audet, P. Toward mapping the effective elastic thickness of planetary lithospheres from a spherical wavelet analysis of gravity and topography. *Phys. Earth Planet. Inter.* **2014**, *226*, 48–82. [CrossRef]
24. Lu, Z.; Li, C.-F.; Zhu, S.; Audet, P. Effective elastic thickness over the Chinese mainland and surroundings estimated from a joint inversion of Bouguer admittance and coherence. *Phys. Earth Planet. Inter.* **2020**, *301*, 106456. [CrossRef]
25. Mora-Páez, H.; Kellogg, J.N.; Freymueller, J.T.; Mencin, D.; Fernandes, R.M.S.; Diederix, H.; LaFemina, P.; Cardona-Piedrahita, L.; Lizarazo, S.; Peláez-Gaviria, J.-R.; et al. Crustal deformation in the northern Andes—A new GPS velocity field. *J. S. Am. Earth Sci.* **2019**, *89*, 76–91. [CrossRef]
26. Cortés, M.; Angelier, J. Current states of stress in the northern Andes as indicated by focal mechanisms of earthquakes. *Tectonophysics* **2005**, *403*, 29–58. [CrossRef]
27. Cortés, M.; Colletta, B.; Angelier, J. Structure and tectonics of the central segment of the Eastern Cordillera of Colombia. *J. S. Am. Earth Sci. Tecton. Evol. Colomb. Andes* **2006**, *21*, 437–465. [CrossRef]
28. Restrepo, J.J.; Toussaint, J.F. Terranes and Continental Accretion in the Colombian Andes. *Epis. J. Int. Geosci.* **1988**, *11*, 189–193. [CrossRef]
29. Redwood, S.D. The Geology of the Panama-Chocó Arc. In *Geology and Tectonics of Northwestern South America: The Pacific-Caribbean-Andean Junction*; Cediel, F., Shaw, R.P., Eds.; Springer International Publishing: Cham, Switzerland, 2019; pp. 901–932. [CrossRef]
30. Taboada, A.; Rivera, L.A.; Fuenzalida, A.; Cisternas, A.; Philip, H.; Bijwaard, H.; Olaya, J.; Rivera, C. Geodynamics of the northern Andes: Subductions and intracontinental deformation (Colombia). *Tectonics* **2000**, *19*, 787–813. [CrossRef]

31. Suter, F.; Sartori, M.; Neuwerth, R.; Gorin, G. Structural imprints at the front of the Chocó-Panamá indenter: Field data from the North Cauca Valley Basin, Central Colombia. *Tectonophysics* **2008**, *460*, 134–157. [CrossRef]
32. Cortés, M.; Angelier, J.; Colletta, B. Paleostress evolution of the northern Andes (Eastern Cordillera of Colombia): Implications on plate kinematics of the South Caribbean region. *Tectonics* **2005**, *24*, TC1008. [CrossRef]
33. Trenkamp, R.; Kellogg, J.N.; Freymueller, J.T.; Mora, H.P. Wide plate margin deformation, southern Central America and northwestern South America, CASA GPS observations. *J. S. Am. Earth Sci.* **2002**, *15*, 157–171. [CrossRef]
34. Veloza, G.; Styron, R.; Taylor, M.; Mora, A. Open-source archive of active faults for northwest South America. *GSAT* **2012**, *22*, 4–10. [CrossRef]
35. Pennington, W.D. Subduction of the Eastern Panama Basin and seismotectonics of northwestern South America. *J. Geophys. Res. Solid Earth* **1981**, *86*, 10753–10770. [CrossRef]
36. Cediel, F.; Shaw, R.P.; Cáceres, C. Tectonic Assembly of the Northern Andean Block. In *The Circum-Gulf of Mexico and the Caribbean: Hydrocarbon Habitats, Basin Formation and Plate Tectonics*; Bartolini, C., Buffler, R.T., Blickwede, J.F., Eds.; American Association of Petroleum Geologists: Tulsa, OK, USA, 2003. [CrossRef]
37. Backé, G.; Dhont, D.; Hervouët, Y. Spatial and temporal relationships between compression, strike-slip and extension in the Central Venezuelan Andes: Clues for Plio-Quaternary tectonic escape. *Tectonophysics* **2006**, *425*, 25–53. [CrossRef]
38. Grösser, J.R. Geotectonic evolution of the Western Cordillera of Colombia: New aspects from geochemical data on volcanic rocks. *J. S. Am. Earth Sci.* **1989**, *2*, 359–369. [CrossRef]
39. Gómez, J.; Núñez–Tello, A.; Mateus–Zabala, D.; Alcárcel–Gutiérrez, F.A.; Lasso–Muñoz, R.M.; Marín–Rincón, E.; Marroquín–Gómez, M.P. Physiographic and geological setting of the Colombian territory. In *The Geology of Colombia, Volume 1 Proterozoic–Paleozoic*; Gómez, J., Mateus–Zabala, D., Eds.; Publicaciones Geológicas Especiales 35; Servicio Geológico Colombiano: Bogotá, Colombia, 2020; pp. 1–16. [CrossRef]
40. Cardona, A.; Valencia, V.A.; Bayona, G.; Duque, J.; Ducea, M.; Gehrels, G.; Jaramillo, C.; Montes, C.; Ojeda, G.; Ruiz, J. Early-subduction-related orogeny in the northern Andes: Turonian to Eocene magmatic and provenance record in the Santa Marta Massif and Rancheria Basin, northern Colombia. *Terra Nova* **2011**, *23*, 26–34. [CrossRef]
41. Parra, M.; Echeverri, S.; Patiño, A.M.; Ramírez, J.C.; Mora, A.; Sobel, E.R.; Almendral, A.; Pardo–Trujillo, A. Cenozoic evolution of the Sierra Nevada de Santa Marta, Colombia. In *The Geology of Colombia, Volume 3 Paleogene–Neogene*; Gómez, J., Mateus–Zabala, D., Eds.; Publicaciones Geológicas Especiales 37; Servicio Geológico Colombiano: Bogotá, Colombia, 2020; pp. 185–213. [CrossRef]
42. Montes, C.; Guzman, G.; Bayona, G.; Cardona, A.; Valencia, V.; Jaramillo, C. Clockwise rotation of the Santa Marta massif and simultaneous Paleogene to Neogene deformation of the Plato-San Jorge and Cesar-Ranchería basins. *J. S. Am. Earth Sci. Sierra Nev. Santa Marta Adjac. Basins* **2010**, *29*, 832–848. [CrossRef]
43. Mantilla-Pimiento, A.M.; Jentzsch, G.; Kley, J.; Alfonso-Pava, C. Configuration of the Colombian Caribbean Margin: Constraints from 2D Seismic Reflection data and Potential Fields Interpretation. In *Subduction Zone Geodynamics*; Lallemand, S., Funiciello, F., Eds.; Springer: Berlin/Heidelberg, Germany, 2009; pp. 247–272. [CrossRef]
44. Toto, E.A.; Kellogg, J.N. Structure of the Sinu-San Jacinto fold belt—An active accretionary prism in northern Colombia. *J. S. Am. Earth Sci.* **1992**, *5*, 211–222. [CrossRef]
45. Duque-Caro, H. Major Structural Elements and Evolution of Northwestern Colombia. In *Geological and Geophysical Investigations of Continental Margins*; Watkins, J.S., Montadert, L., Dickerson, P.W., Eds.; American Association of Petroleum Geologists: Tulsa, OK, USA, 1979. [CrossRef]
46. Mora-Bohórquez, J.A.; Ibánez-Mejia, M.; Oncken, O.; de Freitas, M.; Vélez, V.; Mesa, A.; Serna, L. Structure and age of the Lower Magdalena Valley basin basement, northern Colombia: New reflection-seismic and U-Pb-Hf insights into the termination of the central andes against the Caribbean basin. *J. S. Am. Earth Sci.* **2017**, *74*, 1–26. [CrossRef]
47. Mora–Bohórquez, J.A.; Oncken, O.; Le Breton, E.; Ibañez–Mejia, M.; Veloza, G.; Mora, A.; Vélez, V.; De Freitas, M. Formation and evolution of the Lower Magdalena Valley Basin and San Jacinto fold belt of northwestern Colombia: Insights from Upper Cretaceous to recent tectono–stratigraphy. In *The Geology of Colombia, Volume 3 Paleogene–Neogene*; Gómez, J., Mateus–Zabala, D., Eds.; Publicaciones Geológicas Especiales 37; Servicio Geológico Colombiano: Bogotá, Colombia, 2020; pp. 21–66. [CrossRef]
48. Bernal-Olaya, R.; Mann, P.; Vargas, C.A. Earthquake, Tomographic, Seismic Reflection, and Gravity Evidence for a Shallowly Dipping Subduction Zone beneath the Caribbean Margin of Northwestern Colombia. In *Petroleum Geology and Potential of the Colombian Caribbean Margin*; Bartolini, C., Mann, P., Eds.; American Association of Petroleum Geologists: Tulsa, OK, USA, 2015. [CrossRef]
49. de Almeida, F.F.M.; Hasui, Y.; de Brito Neves, B.B.; Fuck, R.A. Brazilian structural provinces: An introduction. *Earth-Sci. Rev.* **1981**, *17*, 1–29. [CrossRef]
50. Tassinari, C.C.G.; Macambira, M.J.B. Geochronological provinces of the Amazonian Craton. *Epis. J. Int. Geosci.* **1999**, *22*, 174–182. [CrossRef]
51. Moyano-Nieto, I.E.; Prieto, G.A.; Ibañez-Mejia, M. Tectonic domains in the NW Amazonian Craton from geophysical and geological data. *Precambrian Res.* **2022**, *377*, 106735. [CrossRef]

52. Ibañez–Mejia, M.; Cordani, U.G. Zircon U–Pb geochronology and Hf–Nd–O isotope geochemistry of the Paleo– to Mesoproterozoic basement in the westernmost Guiana Shield. In *The Geology of Colombia, Volume 1 Proterozoic–Paleozoic*; Gómez, J., Mateus–Zabala, D., Eds.; Publicaciones Geológicas Especiales 35; Servicio Geológico Colombiano: Bogotá, Colombia, 2020; pp. 65–90. [CrossRef]
53. Kirby, J.F. Which wavelet best reproduces the Fourier power spectrum? *Comput. Geosci.* **2005**, *31*, 846–864. [CrossRef]
54. Kirby, J.F.; Swain, C.J. Improving the spatial resolution of effective elastic thickness estimation with the fan wavelet transform. *Comput. Geosci.* **2011**, *37*, 1345–1354. [CrossRef]
55. Kirby, J.F.; Swain, C.J. An accuracy assessment of the fan wavelet coherence method for elastic thickness estimation. *Geochem. Geophys. Geosyst.* **2008**, *9*, 1–27. [CrossRef]
56. Kirby, J.F.; Swain, C.J. A reassessment of spectral T estimation in continental interiors: The case of North America. *J. Geophys. Res. Solid Earth* **2009**, *114*, 1–36. [CrossRef]
57. Amante, C.; Eakins, B.W. *ETOPO1 1 Arc-Minute Global Relief Model: Procedures, Data Sources and Analysis*; NOAA Technical Memorandum NESDIS NGDC-24; NOAA National Centers for Environmental Information: Asheville, NC, USA, 2009; 19p.
58. Bonvalot, S.; Briais, A.; Kuhn, M.; Peyrefitte, A.; Vales, N.; Biancale, R.; Gabalda, G.; Moreaux, G.; Reinquin, F.; Sarrailh, M. *Global Grids: World Gravity Map (WGM2012)*; Bureau Gravimetrique International: Toulouse, France, 2012. [CrossRef]
59. Laske, G.; Masters, G.; Ma, Z.; Pasyanos, M. Update on CRUST1.0—A 1-degree Global Model of Earth's Crust. *Geophys. Res. Abstr.* **2013**, *15*, 2658.
60. Poveda, E.; Monsalve, G.; Vargas, C.A. Receiver functions and crustal structure of the northwestern Andean region, Colombia. *J. Geophys. Res. Solid Earth* **2015**, *120*, 2408–2425. [CrossRef]
61. Poveda, E.; Julià, J.; Schimmel, M.; Perez-Garcia, N. Upper and Middle Crustal Velocity Structure of the Colombian Andes from Ambient Noise Tomography: Investigating Subduction-Related Magmatism in the Overriding Plate. *J. Geophys. Res. Solid Earth* **2018**, *123*, 1459–1485. [CrossRef]
62. Quiroga, D.E.; Currie, C.A.; Pearse, J. Lithosphere Removal in the Sierra Nevada de Santa Marta, Colombia. *J. Geophys. Res. Solid Earth* **2024**, *129*, e2023JB027646. [CrossRef]
63. Monsalve–Bustamante, M.L. The volcanic front in Colombia: Segmentation and recent and historical activity. In *The Geology of Colombia, Volume 4 Quaternary*; Gómez, J., Pinilla–Pachon, A.O., Eds.; Publicaciones Geológicas Especiales 38; Servicio Geológico Colombiano: Bogotá, Colombia, 2020; pp. 97–159. [CrossRef]
64. Koch, C.D.; Delph, J.; Beck, S.L.; Lynner, C.; Ruiz, M.; Hernandez, S.; Samaniego, P.; Meltzer, A.; Mothes, P.; Hidalgo, S. Crustal thickness and magma storage beneath the Ecuadorian arc. *J. S. Am. Earth Sci.* **2021**, *110*, 103331. [CrossRef]
65. Ebmeier, S.K.; Elliott, J.R.; Nocquet, J.-M.; Biggs, J.; Mothes, P.; Jarrín, P.; Yépez, M.; Aguaiza, S.; Lundgren, P.; Samsonov, S.V. Shallow earthquake inhibits unrest near Chiles–Cerro Negro volcanoes, Ecuador–Colombian border. *Earth Planet. Sci. Lett.* **2016**, *450*, 283–291. [CrossRef]
66. Bloch, E.; Ibañez-Mejia, M.; Murray, K.; Vervoort, J.; Müntener, O. Recent crustal foundering in the Northern Volcanic Zone of the Andean arc: Petrological insights from the roots of a modern subduction zone. *Earth Planet. Sci. Lett.* **2017**, *476*, 47–58. [CrossRef]
67. Rodríguez, E.E.; Beck, S.L.; Meltzer, A.; Segovia, M.; Ruíz, M.; Hernández, S.; Roecker, S.; Lynner, C.; Koch, C.; Hoskins, M.C.; et al. Seismic imaging of the Ecuadorian forearc and arc from joint ambient noise, local, and teleseismic tomography: Catching the Nazca slab in the act of flattening. *Geophys. J. Int.* **2025**, *241*, 1552–1571. [CrossRef]
68. Vargas, C.A.; Pujades, L.G.; Montes, L. Seismic structure of South-Central Andes of Colombia by tomographic inversion. *Geofísica Int.* **2007**, *46*, 117–127. [CrossRef]
69. Marín-Cerón, M.I.; Leal-Mejía, H.; Bernet, M.; Mesa-García, J. Late Cenozoic to Modern-Day Volcanism in the Northern Andes: A Geochronological, Petrographical, and Geochemical Review. In *Geology and Tectonics of Northwestern South America: The Pacific-Caribbean-Andean Junction*; Cediel, F., Shaw, R.P., Eds.; Springer International Publishing: Cham, Switzerland, 2019; pp. 603–648. [CrossRef]
70. Pérez-Gussinyé, M.; Lowry, A.R.; Phipps Morgan, J.; Tassara, A. Effective elastic thickness variations along the Andean margin and their relationship to subduction geometry. *Geochem. Geophys. Geosystems* **2008**, *2*, 1–21. [CrossRef]
71. Mojica Boada, M.J.; Poveda, E.; Tary, J.B. Lithospheric and Slab Configurations from Receiver Function Imaging in Northwestern South America, Colombia. *J. Geophys. Res. Solid Earth* **2022**, *127*, e2022JB024475. [CrossRef]
72. Avellaneda-Jiménez, D.S.; Monsalve, G.; León, S.; Gómez-García, A.M. Insights into Moho depth beneath the northwestern Andean region from gravity data inversion. *Geophys. J. Int.* **2022**, *229*, 1964–1977. [CrossRef]
73. Montes, C.; Hatcher, R.D.; Restrepo-Pace, P.A. Tectonic reconstruction of the northern Andean blocks: Oblique convergence and rotations derived from the kinematics of the Piedras–Girardot area, Colombia. *Tectonophysics* **2005**, *399*, 221–250. [CrossRef]
74. Nie, J.; Horton, B.K.; Saylor, J.E.; Mora, A.; Mange, M.; Garzione, C.N.; Basu, A.; Moreno, C.J.; Caballero, V.; Parra, M. Integrated provenance analysis of a convergent retroarc foreland system: U–Pb ages, heavy minerals, Nd isotopes, and sandstone compositions of the Middle Magdalena Valley basin, northern Andes, Colombia. *Earth-Sci. Rev.* **2012**, *110*, 111–126. [CrossRef]

75. Pachón-Parra, L.F.; Mann, P.; Cardozo, N. Regional subsurface mapping and 3D flexural modeling of the obliquely converging Putumayo foreland basin, southern Colombia. *Interpretation* **2020**, *8*, ST15–ST48. [CrossRef]
76. Kroonenberg, S.B.; Reeves, C.V. Geology and petroleum potential, Vaupés-Amazonas Basins, Colombia. In Petroleum Geology of Colombia; Cediel, F., Ed.; Universidad EAFIT, Medellín, Colombia, 2011; 92p.
77. Feng, M.; van der Lee, S.; Assumpção, M. Upper mantle structure of South America from joint inversion of waveforms and fundamental mode group velocities of Rayleigh waves. *J. Geophys. Res. Solid Earth* **2007**, *112*, 1–16. [CrossRef]
78. Chagas de Melo, B.; Lebedev, S.; Celli, N.L.; Gibson, S.; de Laat, J.I.; Assumpção, M. The lithosphere of South America from seismic tomography: Structure, evolution, and control on tectonics and magmatism. *Gondwana Res.* **2025**, *138*, 139–167. [CrossRef]
79. Rockwell, T.K.; Bennett, R.A.; Gath, E.; Franceschi, P. Unhinging an indenter: A new tectonic model for the internal deformation of Panama. *Tectonics* **2010**, *29*, 1–10. [CrossRef]
80. Mantovani, M.S.M.; de Freitas, S.R.C.; Shukowsky, W. Tidal gravity anomalies as a tool to measure rheological properties of the continental lithosphere: Application to the South American Plate. *J. S. Am. Earth Sci.* **2001**, *14*, 1–14. [CrossRef]
81. Mantovani, M.S.M.; Shukowsky, W.; de Freitas, S.R.C.; Brito Neves, B.B. Lithosphere mechanical behavior inferred from tidal gravity anomalies: A comparison of Africa and South America. *Earth Planet. Sci. Lett.* **2005**, *230*, 397–412. [CrossRef]
82. Cerón, J.F.; Kellogg, J.N.; Ojeda, G.Y. Basement configuration of the northwestern South America-Caribbean margin from recent geophysical data. *CT&F-Cienc. Tecnol. Futuro* **2007**, *3*, 25–49. [CrossRef]
83. Londono, J.; Lorenzo, J.M.; Ramirez, V. Lithospheric Flexure and Related Base-Level Stratigraphic Cycles in Continental Foreland Basins: An Example from the Putumayo Basin, Northern Andes. In *Tectonics and Sedimentation: Implications for Petroleum Systems*; Gao, D., Ed.; American Association of Petroleum Geologists: Tulsa, OK, USA, 2013. [CrossRef]
84. Lu, Z.; Audet, P.; Li, J.; Zhang, T.; Li, C.-F. Strength of continental lithosphere governed by the time since the last orogeny. *Earth Planet. Sci. Lett.* **2024**, *643*, 118894. [CrossRef]
85. Tesauro, M.; Kaban, M.K.; Cloetingh, S.A.P.L. Global strength and elastic thickness of the lithosphere. *Glob. Planet. Change* **2012**, *90–91*, 51–57. [CrossRef]
86. Mareschal, J.C.; Jaupart, C.; Rolandone, F.; Gariépy, C.; Fowler, C.M.R.; Bienfait, G.; Carbonne, C.; Lapointe, R. Heat flow, thermal regime, and elastic thickness of the lithosphere in the Trans-Hudson Orogen. *Can. J. Earth Sci.* **2005**, *42*, 517–532. [CrossRef]
87. Zamani, A.; Samiee, J.; Kirby, J.F. The effective elastic thickness of the lithosphere in the collision zone between Arabia and Eurasia in Iran. *J. Geodyn.* **2014**, *81*, 30–40. [CrossRef]
88. Lucazeau, F. Analysis and Mapping of an Updated Terrestrial Heat Flow Data Set. *Geochem. Geophys. Geosystems* **2019**, *20*, 4001–4024. [CrossRef]
89. Debayle, E.; Dubuffet, F.; Durand, S. An automatically updated S-wave model of the upper mantle and the depth extent of azimuthal anisotropy. *Geophys. Res. Lett.* **2016**, *43*, 674–682. [CrossRef]
90. Maggi, A.; Jackson, J.A.; McKenzie, D.; Priestley, K. Earthquake focal depths, effective elastic thickness, and the strength of the continental lithosphere. *Geology* **2000**, *28*, 495–498. [CrossRef]
91. Agurto-Detzel, H.; Assumpção, M.; Bianchi, M.; Pirchiner, M. Intraplate seismicity in mid-plate South America: Correlations with geophysical lithospheric parameters. *Geol. Soc. Lond. Spec. Publ.* **2017**, *432*, 73–90. [CrossRef]
92. International Seismological Centre. ISC-GEM Earthquake Catalogue. 2023. Available online: https://www.isc.ac.uk/iscgem/download.php. (accessed on 25 January 2025).
93. Chen, B.; Chen, C.; Kaban, M.K.; Du, J.; Liang, Q.; Thomas, M. Variations of the effective elastic thickness over China and surroundings and their relation to the lithosphere dynamics. *Earth Planet. Sci. Lett.* **2013**, *363*, 61–72. [CrossRef]
94. Burov, E.B.; Watts, A.B. The long-term strength of continental lithosphere: "Jelly sandwich" or "crème brûlée"? *GSA Today* **2006**, *16*, 4–10. [CrossRef]
95. Audet, P. PlateFlex: Software for Mapping the Elastic Thickness of the Lithosphere. 2019. Available online: https://zenodo.org/records/3576803 (accessed on 9 July 2024).
96. Wessel, P.; Luis, J.F.; Uieda, L.; Scharroo, R.; Wobbe, F.; Smith, W.H.F.; Tian, D. The Generic Mapping Tools Version 6. *Geochem. Geophys. Geosystems* **2019**, *20*, 5556–5564. [CrossRef]

Disclaimer/Publisher's Note: The statements, opinions and data contained in all publications are solely those of the individual author(s) and contributor(s) and not of MDPI and/or the editor(s). MDPI and/or the editor(s) disclaim responsibility for any injury to people or property resulting from any ideas, methods, instructions or products referred to in the content.